JOURNAL OF SOLID STATE CHEMISTRY 116, 240–248 (1995)

An Electron Microscope Investigation of the Bi_2TeO_5–$Bi_2Te_2O_7$ Phase Region

B. Frit, D. Mercurio, and B. H. Parry

Laboratoire de Chimie Minérale Structurale, Université de Limoges, 123 Ave Albert Thomas, 87060 Limoges Cedex, France

and

G. Harburn, R. P. Williams, and R. J. D. Tilley*

*Department of Physics and *School of Engineering, University of Wales, PO Box 925, Newport Road, Cardiff CF2 1YF, United Kingdom*

Received November 5, 1993; in revised form August 15, 1994; accepted September 23, 1994

The nonstoichiometric phase region occurring between Bi_2TeO_5 and $Bi_2Te_2O_7$ has been studied by electron microscopy and diffraction. The electron diffraction patterns are interpreted in terms of a shift lattice. The complexity of the phase region is defined by a constant value of the parameter ϵ equal to $\frac{1}{8}$ and a smooth variation of the parameter β from 24.7 to 9.9 as both composition and temperature of preparation varied. The microstructures of the materials giving rise to these diffraction patterns are presented and discussed in terms of shift lattices, intergrowths, and modulated structures.

INTRODUCTION

In previous publications, Mercurio and co-workers have reported on the phases to be found between Bi_2TeO_5 and $Bi_2Te_2O_7$ in the Bi_2O_3–TeO_2 system (1–4). This composition region consists of a complex fluorite-structure-related phase range. The electron-diffraction patterns from across most of this region form a continuum, the majority being incommensurate. The composition range has therefore been interpreted in the past as containing a large number of ordered structures of the type described by Anderson as "infinitely-adaptive" (5) which may be considered as a subgroup of the class of modulated structures (2, 6).

Whilst it is now becoming possible to treat modulated structures rigorously from a crystallographic point of view using higher dimensional space groups, considerable insight into the crystal chemistry of such systems can be obtained via a construction called the shift lattice (7, 8). In this paper, we apply the method to the diffraction patterns found in the Bi_2TeO_5–$Bi_2Te_2O_7$ phase region. Additionally, we present electron micrographs of the microstructures which occur that have not been published previously. These results are discussed in terms of shift lattices, intergrowths, and modulated-structure models.

EXPERIMENTAL

Sample preparation and characterization via X-ray diffraction and electron diffraction have been described in detail in previous publications (1–4). Electron micrographs were obtained using a Jeol 200CX electron microscope fitted with a top entry goniometer stage capable of $\pm 10°$ tilt. Samples for electron microscopy were prepared by crushing selected samples under *n*-butanol in an agate mortar and allowing a drop of the resultant suspension to dry on a holey carbon support film mounted on a conventional copper grid. Correctly oriented crystal fragments which projected over holes in the underlying film were photographed at a direct magnification of 500,000×.

RESULTS AND INTERPRETATION

Diffraction Patterns

The electron diffraction patterns from the phase range of interest have been described in detail previously. In general, they consist of a square array of bright spots which correspond to the {200} type reflections of the fluorite subcell together with characteristic groups of superlattice spots lying along the b^* axis of the fluorite subcell, as shown in Fig. 1a. The intensity of the superlattice spots rises to a maximum at a point between $\frac{1}{4}$ and $\frac{1}{3}$ d^*_{020} and again between $\frac{2}{3}$ and $\frac{3}{4}$ d^*_{020}, where d^*_{020} is defined as the

0022-4596/95 $6.00

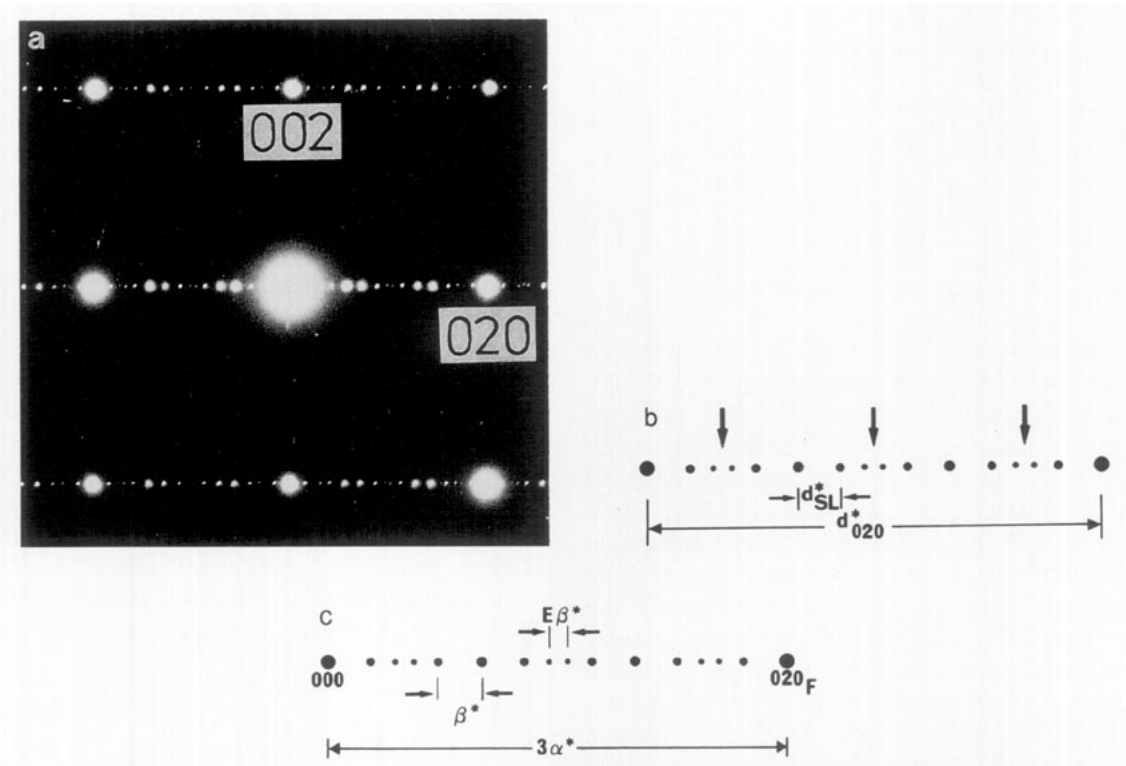

FIG. 1. (a) Electron diffraction pattern typical of the incommensurate phase region taken from a sample of composition $Bi_2O_3 : 1.7TeO_2$. The bright spots correspond to the {200} cubic fluorite subcell reflections. (b). Diagram of the central row of a diffraction showing the relevant reciprocal lattice parameters. The arrows indicate the positions of spacing anomalies in incommensurate patterns. (c). As in (b) but showing the shift lattice parameters.

distance between the 000 and 020 sublattice reflection, as shown in Fig. 1b. Sometimes these rows of spots are inclined at a small angle to the b^* axis. The number, spacing, and intensities of the superlattice spots vary greatly, but despite this complexity the spots were always sharp and no trace of diffuse scattering or streaking has been observed.

In order to characterize the extent of the apparent unit cell in the direction parallel to the b axis, an experimental multiplicity l was determined (4). This parameter was defined as the ratio d^*_{020}/d^*_{SL}, where d^*_{SL} is the separation of two adjacent superlattice spots measured near to a maximum in intensity referred to above, as shown in Fig. 1b. The results revealed that the superstructure evolved both with composition and with the temperature at which the samples were prepared, and that the diffraction patterns were mostly incommensurate. This feature could sometimes be seen directly as anomalous spacings occurring at the three points between two adjacent fluorite subcell reflections, shown by arrows in Fig. 1b.

In the past, these diffraction patterns have been interpreted in terms of intergrowths of two structure types (4). These have often been considered as discrete slabs of identical structure, such as occur in crystallographic shear phases and, as such, the diffraction patterns have been well analyzed (9). However, it appears that new light can be shed on the crystal chemistry of these phases if interpretation is made in terms of a recently introduced formalism called the shift lattice (7, 8), which we therefore present here. The one-dimensional shift lattice and its use in the analysis of electron diffraction patterns have been described in detail elsewhere (7, 8). A brief synopsis is included in the Appendix. Figure 1c defines the reciprocal shift lattice dimensions involved. The shift lattice parameter, β, is expressed in units of $a_F/2$, where a_F is the fluorite unit cell parameter, approximately 0.5 nm. Thus β is the same numerically as the multiplicity, l, used previously (4). Figure 1c shows that we have taken $3\alpha^*$ to be equal to d^*_{020}, giving a value of α of $3d_{020}$, which is equal to $3a_{F/2}$, Recall that the maximum intensity within each of the groups of superlattice spots moves with composition as described above. However, at this point it seems reasonable to take $3\alpha^* = d^*_{020}$ as the nonstoichiometric phase range of interest appears to derive from a Bi_2TeO_5 parent structure and as only two clusters of spots are found in the 000–020_F interval. This point is taken up again in the Discussion.

Within this framework, inspection and measurement of a large number of diffraction patterns showed, without any exception, that they could be interpreted as arising

TABLE 1
Values of the Shift Lattice Parameter β[a]

Temperature (°C)	Maximum β	Minimum β
650	19.1	9.9
700	22.3	10.2
730	22.3	11.3
800	24.7	17.7

[a] Taken from (4); note that l in (4) is equivalent to β.

from a shift lattice with $\varepsilon = \frac{2}{3} \pm 0.025$. It was found that β varied in a continuous and smooth fashion over the composition range studied from a maximum value of 24.7 ± 0.5 in the phase region closest to Bi_2TeO_5 which showed superlattice reflections, to a minimum value of 9.9 ± 0.5 in the phase region closest to $Bi_2Te_2O_7$. These are summarized in Table 1. Inspection of the diffraction patterns (see (3, 4) for examples) showed that the envelope of the superlattice spots was generally narrower for the samples with closely spaced superlattice spots and wider for those with larger superlattice spot spacings. The value of w, i.e., the lengths of the blocks of lattice fragments, is obtained by estimating the point at which this envelope reaches its first zero. Such an estimate is difficult to make although it is clear that a large value of β is associated with a large value of w, and vice versa. Within the precision of the estimate of w, typically $\pm 10\%$, it seemed that the value of $(\beta - w)$ remained constant and to have a value close to 5 in units of $\alpha/3$.

These experimental parameters can be used to construct shift lattices yielding diffraction patterns characteristic of those found across the phase range. Schematic diagrams of four shift lattices and diffraction patterns constructed with various β values are shown in Figs. 2 and 3. The horizontal lines represent the envelope function (of value unity under the line and zero elsewhere) by which the comb function, whose tooth spacing is α, is multiplied. Combs under adjacent envelopes are displaced with respect to each other by $\varepsilon = 2\alpha/3$. This means (for $\varepsilon = \frac{2}{3}$) that the distance between the right-hand tooth in one envelope and the left-hand tooth in the envelope to its right can be only separated by $\alpha + 2\alpha/3 = 5\alpha/3$ or $2\alpha + 2\alpha/3 = 8\alpha/3$ or $11\alpha/3$ or $14\alpha/3$, etc. However, the additional restriction that $\beta - w = 5\alpha/3$ precludes all of the above possibilities other than $5\alpha/3$ and $8\alpha/3$, so that with these parameters no other possibilities exist. Figure 2 therefore shows that the shift lattices consist of fragments of comb, each fragment being separated from its neighbor either by a distance of either $5\alpha/3$ or $8\alpha/3$.

The spacing between the lattice fragments is dependent upon the relative "phase" of the fragments with respect to

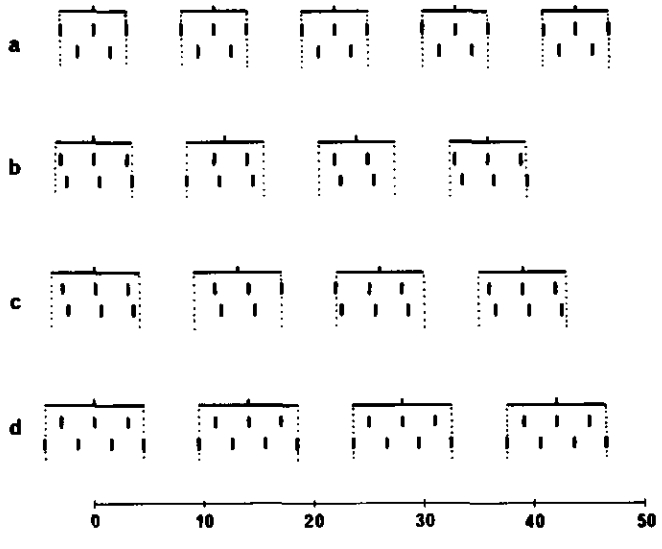

FIG. 2. Shift lattices constructed with the parameters (a) $\beta = 11$, $w = 6$, $[3^25)]$, and $[(38)]$; (b) $\beta = 12$, $w = 7$, $[(3^28)(38)^2]$, and $[(3^25)(3^28)(38)]$; (c) $\beta = 13$, $w = 8$, $[(3^28)^2(3^25)]$, and $[(3^28)^2(38)]$; (d) $\beta = 14$, $w = 9$, $[(3^28)]$, and $[(3^35)]$. The parameter ε is equal to $\frac{2}{3}$ and α equal to 3 in each case.

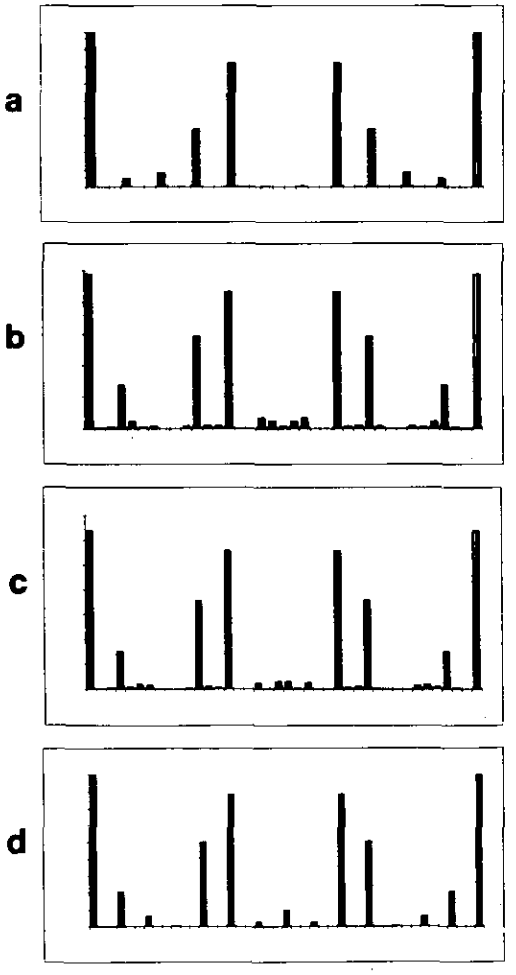

FIG. 3. The calculated diffraction patterns from the shift lattices shown as Figs. 2a–2d are shown in (a)–(d), respectively.

TABLE 2
Calculated Stacking Sequences for Given Values of β and w

β	w	Sequence	
11	6	[38]	[$3^2$5]
11.2	6.2	[$(38)^{14}(3^28)$]	
11.5	6.5	[$(38)^5(3^28)$]	
11.6	6.6	[$(38)^4(3^28)$]	
11.7	6.7	[$(38)^4(3^28)\{(38)^3(3^28)\}^5$]	
11.8	6.8	[$\{(38)^3(3^28)\}^2(38)^2(3^28)$]	
11.9	6.9	[$(38)^3(3^28)\{(38)^2(3^28)\}^2$]	
12.0	7.0	[$(38)^2(3^28)$]	
14	9	[$3^2$8]	[$3^3$5]
17	12	[$3^3$8]	[$3^4$5]
20	15	[$3^4$8]	[$3^5$5]
23	18	[$3^5$8]	[$3^6$5]

an arbitrary origin. In the majority of cases, the separation between lattice fragments is $8\alpha/3$. However, if the right-hand delta function in a group falls exactly at the extremity of the envelope function, the separation of the groups will be $5\alpha/3$. This converts a sequence of ...38... into a sequence of ...335... . These alternatives are shown in Figs. 2b and 2c. In the case where the width w is equal to $n\alpha$ (where n is an integer), this is repeated in each group, so that separations of 8 are completely eliminated. This situation is illustrated in Figs. 2a and 2d. No other possibilities arise.

Some of the sequences generated from the experimental parameters are given in Table 2. These show the two possibilities, with separations $5\alpha/3$ or $8\alpha/3$, for β values from 11 to 23 in steps of 3. Additionally the smaller interval between $\beta = 11$ and $\beta = 12$ is presented in smaller steps for the case when the separation of each fragment is $8\alpha/3$. In this table, the sequence of delta functions is represented by 3 for $3\alpha/3$, or 8 for $8\alpha/3$. A repeat unit is enclosed in square brackets and multiple repeats are denoted by superscripts, as can be seen by a comparison with Fig. 2.

Microstructures

The idealized structure of Bi_2TeO_5, the parent phase of the materials studied here, is shown in Fig. 4. This was examined via electron microscopy as an aid to the interpretation of the modulated phase region. The crystals were found to be beam sensitive and frequently decomposed during observation so that images often showed contrast typical of an amorphous material. No unexpected contrast features were found in crystal regions which did not decompose significantly and image calculations were able to reproduce them satisfactorily.

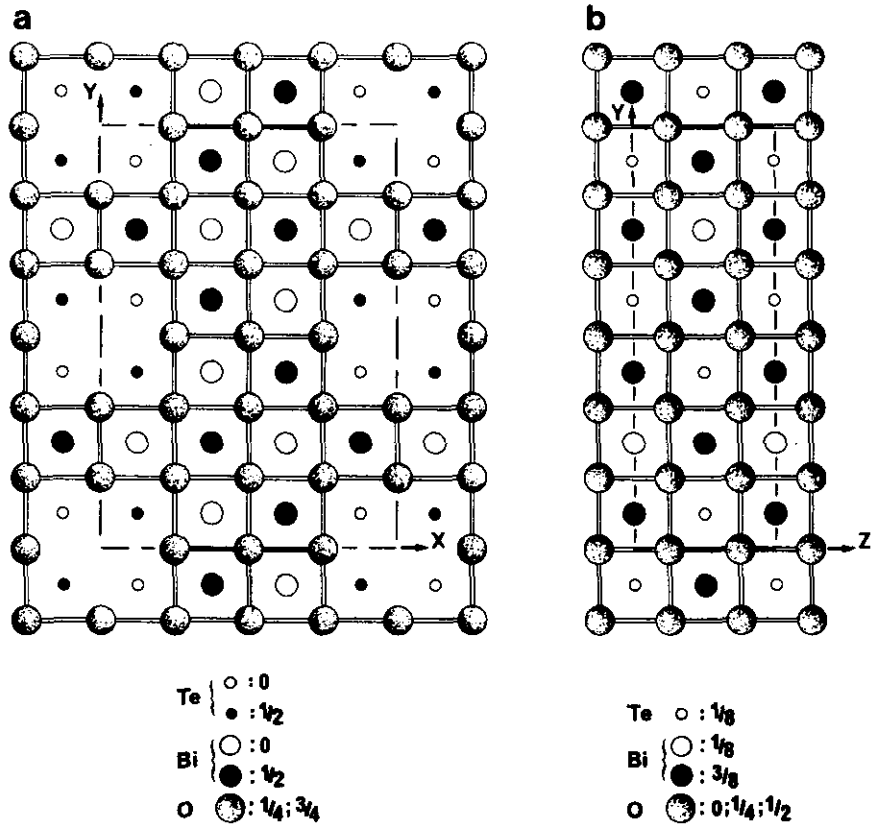

FIG. 4. The idealized crystal structure of Bi_2TeO_5 (a) projected down [001] and (b) projected down [100].

Although crystal decomposition also proved to be a severe problem when images of the preparations from the middle part of the composition range were sought, it was immediately apparent that the phase range was not made up of a series of intergrowths built of coherently joined slabs of structure. Most images obtained from undecomposed crystal regions came from thicker parts and consisted of parallel fringes running perpendicular to the *b*

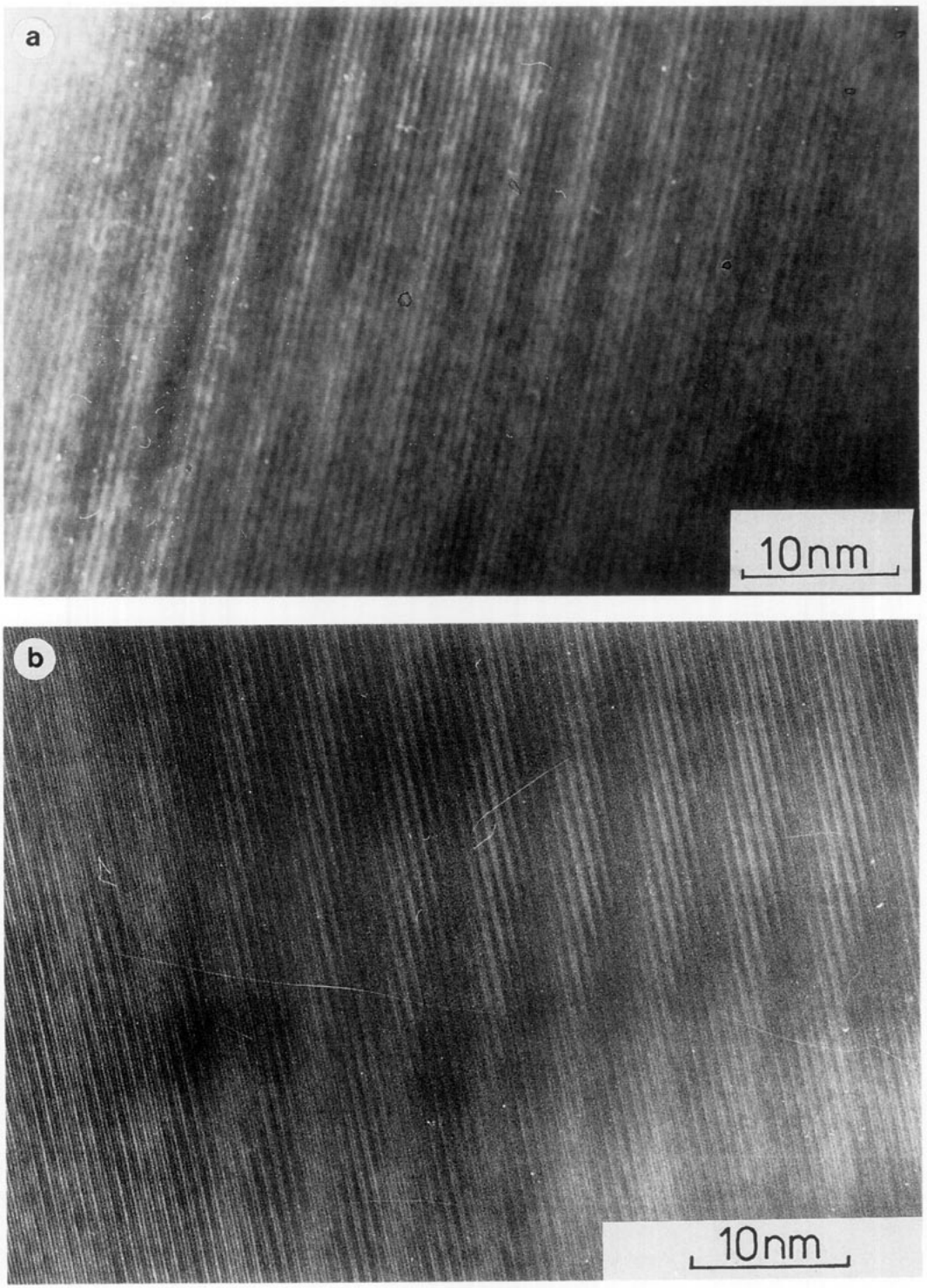

FIG. 5. Electron micrographs showing broad fringes of relatively low contrast separated by a distance β. In (a) these are parallel to the subcell fringes, while in (b) they are at an angle to the subcell fringes which have a spacing of $a_{F/2}$.

axis with a spacing of $a_{F/2}$. The contrast variation across each image was modulated by a set of wide, regularly spaced broad fringes of low relative contrast. These normally ran parallel to the narrow $a_{F/2}$ fringes, as shown in Fig. 5a, but at times were found to lie at an angle to these subcell fringes, as shown in Fig. 5b. These two situations correspond to diffraction patterns with rows of superlattice spots running strictly parallel to b^* and at a small angle to b^*, respectively. The wavelength of the broad fringes corresponded to the parameter β and so evolved in spacing across the composition range studied. Toward the Bi_2TeO_5-rich side of the phase region, fragments were found in which part of the crystal showed contrast typical of Bi_2TeO_5 while contiguous regions showed the regular modulations in contrast associated with the intermediate phases, but no sharp boundaries between the two regions could be imaged. An example is shown in Fig. 6.

Interpretation of the underlying atomic positions which gave rise to the diffuse fringes was difficult. In the thicker parts of the crystals the contrast was complex, while in the thinner parts decomposition frequently destroyed such variation, leaving only the fluorite subcell contrast. Nevertheless, images were occasionally found which revealed a microstructure consisting of a stacking of different structural units. Figure 7 shows a crystal fragment from a sample of overall composition Bi_2O_3 : $1.7TeO_2$ heated at 700°C. The diffraction pattern from this crystal, shown as that in Fig. 1a, indicated that β was 12.8 and that the pattern was incommensurate. Pairs of slabs with a contrast similar to that expected from Bi_2TeO_5 are shown by arrows. These were often separated by slabs of eight fringes, giving a repetition of $14a_{F/2}$. However, the contrast along these latter strips varies so that in some regions they appear as uniform slabs of 8 fringes whereas sometimes this contrast is made up of an extra slab of Bi_2TeO_5, i.e., a contrast of 3 plus 5, best seen in Fig. 7b.

DISCUSSION

The diffraction patterns from the phases investigated here conform to those expected from a shift lattice with a constant value of $\frac{2}{3}$ for the shift parameter of ε and a smoothly varying value for the parameters β and w. These can be used to construct all possible stacking sequences which can arise as β is varied over the range found and beyond in a mechanical fashion. Two features appear. Firstly, each value of β gives rise to a stacking sequence consisting of groups of units of separation α separated by strips of width $5\alpha/3$ or $8\alpha/3$. Values of β which are nonintegral give more complex sequences with longer repeat units, and it is not difficult to construct perfectly ordered sequences which never repeat. That is, despite the fact that the sequences are ordered and totally predictable from a knowledge of the shift lattice input parameters, the structure does not possess a unit cell in the crystallographic sense, the repeat distance being infinity. The sequences determined for simple values of β are in perfect agreement with sequences suggested empirically earlier (4), but the construction of the shift lattice shows that only spaces of width $5\alpha/3$ and $8\alpha/3$ can occur between the sequences of α. In particular, in order to have a separation of $4\alpha/3$ it would be necessary to have a value of ε

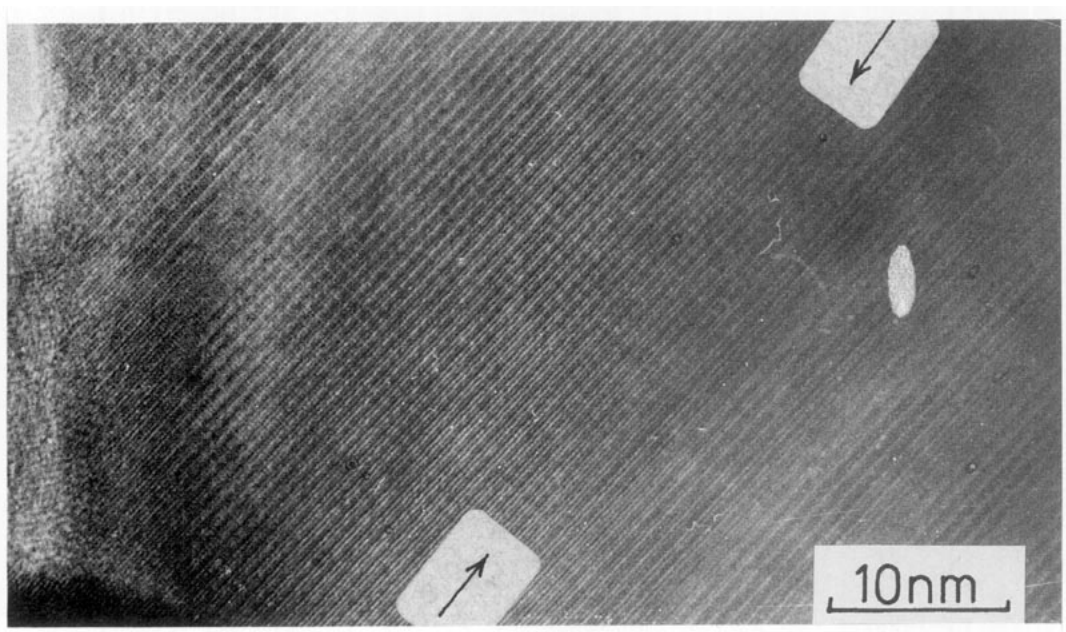

FIG. 6. Electron micrograph of a crystal showing contrast typical of Bi_2TeO_5 on the left of the image and low contrast modulations on the right. The boundary between the two regions is shown by arrows.

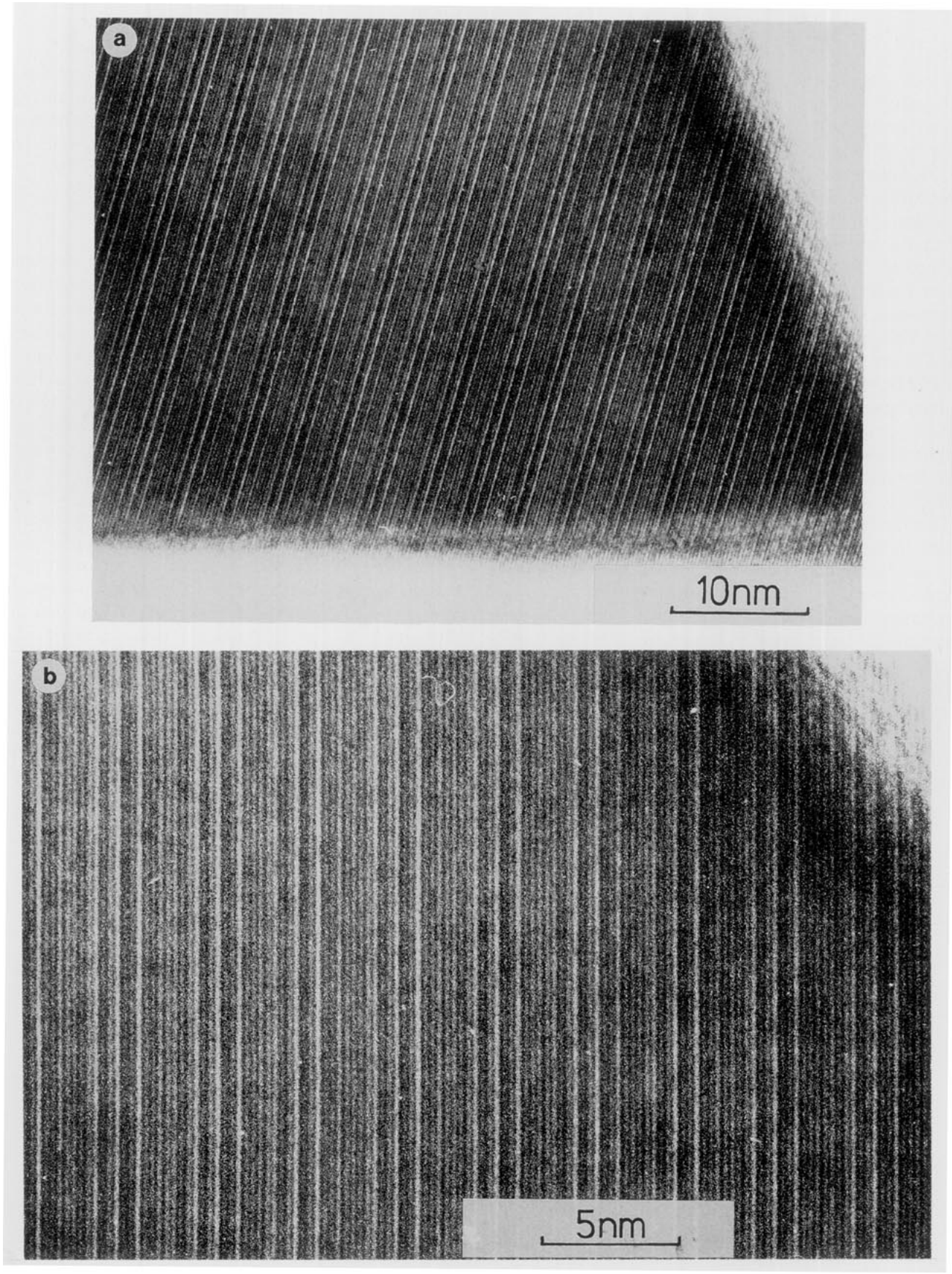

FIG. 7. (a) Electron micrograph showing an almost ordered intergrowth of units [3, 3, 8] $a_{F/2}$ from a sample of overall composition $Bi_2O_3 : 1.7TeO_2$. In many cases the units of 8 appear to be disproportionating into units of [5, 3], as can be seen more clearly in the enlargement (b). The diffraction pattern is shown as that in Fig. 1a.

equal to $\frac{1}{3}$. Compared to previous descriptions of this phase range, using multiplicity values, a considerable simplification has been achieved. The whole spectrum of diffraction patterns can be characterized by smoothly varying the connected parameters β and w, and by two constants $\varepsilon = \frac{2}{3}$ and $\beta - w = 5$, rather than by a chaotic sequence of multiplicity values.

The shift lattice construction does not, in general, produce a structure in the crystallographic sense, but it does reveal how the structure can evolve with, e.g., composition. As no structures have yet been determined for these long unit cell phases, the sequences derived by application of the shift lattice can be linked to crystallographic structures only indirectly. To do this, we consider the one relevant structure that has been solved to date, that of Bi_2TeO_5 (1). The dominant motif in this structure is the presence of columns of oxygen vacancies separated along the b axis by a distance of $3a_{F/2}$. The sequence of metal atom planes along the same axis in the unit cell is ... Bi, (Bi + Te), (Bi + Te), Bi, (Bi + Te), (Bi + Te), Bi, ... Because of this structural relationship it is reasonable to suggest that the separation, α, of teeth in the shift lattice should be equated with a half unit cell of Bi_2TeO_5. In the absence of any other structural information, the region of width $5a_{F/2}$ or $8a_{F/2}$, can be considered to consist of planes containing a distribution of Bi and Te atoms, which is different from that in Bi_2TeO_5. If this concept is taken further and the positions of the teeth in Fig. 2 are equated with the planes of Bi atoms in Bi_2TeO_5, then a shift of $\frac{2}{3}$ introduces two extra planes (Bi + Te), to produce the sequence Bi, (Bi + Te), (Bi + Te), (Bi + Te), (Bi + Te), Bi, or five extra planes (Bi + Te) to produce the sequence Bi, (Bi + Te), (Bi + Te), (Bi + Te), (Bi + Te), (Bi + Te), (Bi + Te), (Bi + Te), Bi. The composition is moved toward $Bi_2Te_2O_7$, as required. It may be possible to describe these sequences as an intergrowth of $Bi_2Te_2O_7$ into a matrix which consists of multiples of half unit cells of Bi_2TeO_5. However, as the structure of $Bi_2Te_2O_7$ has not yet been solved in detail, it is more reasonable at the moment to leave this question open.

A final point needs to be clarified with respect to the diffraction patterns. It is known that the position of the subsidiary maxima between the 000 and 020 reflections of the subcell move from about $\frac{1}{3}$ and $\frac{2}{3}\,d^*_{020}$ toward $\frac{1}{4}$ and $\frac{3}{4}d^*_{020}$. The shift lattice construction described above does not reproduce this exactly because we have focused upon the Bi_2TeO_5 part of the lattice and regarded the regions between the fragments of the comb as being empty. In reality this is not so, and these contribute to the overall intensity pattern observed. Should the shift lattice be drawn with these regions emphasized and the regions between them empty, then the overall intensity pattern would rise to maxima at $\frac{1}{4}$ and $\frac{3}{4}d^*_{020}$. Experimentally obtained diffraction patterns, which contain contributions from both of these regions, weighted with respect to the composition, show the smooth transition from one extreme to the other as the overall composition of the sample changes from the Bi_2TeO_5-rich region to the $Bi_2Te_2O_7$-rich region. This again emphasizes that the shift lattice construction is not necessarily a means of producing a crystallographic solution to a structural problem.

The electron micrographs indicate that at an atomic level the structures are not simple intergrowths. The broad fringes with a spacing of β are typical of a modulated structure and sharp contrast changes typical of intergrowth as is found, for example, in the layered perovskites, does not occur. Similarly it is possible to say that across the composition range of the intermediate phases a simple change in the stacking ratio of two different structure types is not taking place. As it is clear that this structure is able to coexist with that of Bi_2TeO_5 it seems reasonable to suppose that it is this latter structure that has been modulated in order to accommodate the change in stoichiometry and that the modulation changes continuously over the phase field of interest. Nevertheless, there is to some extent the suggestion of an intergrowth present as the fringe intensity pattern in, e.g., Fig. 7, suggest an intergrowth of slabs of Bi_2TeO_5 with an undifferentiated structure. However, the contrast, even along a well defined strip of structure as that shown in Fig. 7, often changes from, for example, an 8 fringe repeat to a 3 plus 5 repeat, and it seems that a description in terms of intergrowth between different units of structure is incomplete. Modulation of the structure in addition to that imposed by the intergrowth may be important. A more complete interpretation of contrast must wait for the solution of the structure of $Bi_2Te_2O_7$ and some of these intermediate phases.

APPENDIX: THE SHIFT LATTICE

The one-dimensional shift lattice, of relevance here, is constructed from a set of identical motifs, represented by δ-functions, separated by a distance α along x. This "comb" is constrained to lie within a space of length w. The shift lattice consists of an infinite set of such blocks of comb. Each block is separated from its neighbors by a constant distance β and on passing from one block to its neighbor a shift in the position of the δ-functions of $\varepsilon\alpha$ occurs, where $0 < \varepsilon < 1$. Hence the mth block is shifted by $m\varepsilon\alpha$ compared to that at the origin, $m = 0$. Such constructions are shown in Fig. 2.

The one-dimensional shift lattice can be represented by the function

$$f(x) = \sum_{m=-\infty}^{+\infty} g(x - m\beta)\delta_a(x - m\varepsilon\alpha). \qquad [1]$$

Its Fourier transform is

$$F(u) = \alpha^*\beta^* \sum_{h=-\infty}^{+\infty} G(u - h\alpha^*)\delta_{\beta^*}(u - hE\beta^*), \quad [2]$$

where u is the reciprocal space variable, $\alpha^* = 1/\alpha$, $\beta^* = 1/\beta$, $G(u)$ is the transform of $g(x)$, h is an integer, and

$$E + \varepsilon = \alpha^*/\beta^*.$$

As diffraction patterns are related to their corresponding structures through Fourier transformation, the Fourier transform [2] corresponds to the diffraction pattern generated by the structure [1]. Measurement of the relevant quantities α^*, β^*, and E on a diffraction pattern (cf. Fig. 1) allows the shift lattice, Eq. [1], to be determined.

ACKNOWLEDGMENTS

R.J.D.T. is indebted to the University of Limoges and B.H.P. to the Royal Society of London for financial assistance which has made this collaborative study possible.

REFERENCES

1. D. Mercurio, M. el Farissi, B. Frit, and P. Goursat, *Mater. Chem. Phys.* **9,** 467 (1983).
2. M. el Farissi, D. Mercurio, and B. Frit. *Mater. Chem. Phys.* **16,** 133 (1987).
3. D. Mercurio, B. Frit, G. Harburn, B. H. Parry, R. P. Williams, and R. J. D. Tilley, *Phys. Status Solidi A* **108,** 111 (1988).
4. D. Mercurio, B. H. Parry, B. Frit, G. Harburn, R. P. Williams, and R. J. D. Tilley, *J. Solid State Chem.* **92,** 449 (1991).
5. J. S. Anderson, *J. Chem. Soc. Dalton Trans.*, 1107 (1973).
6. R. L. Withers, *Prog. Cryst. Growth Charact.* **18,** 139 (1989).
7. G. Harburn, R. J. D. Tilley, J. M. Williams, and R. P. Williams, *Nature* **350,** 214 (1991).
8. G. Harburn, R. J. D. Tilley, J. M. Williams, and R. P. Williams, *Proc. R. Soc. London Ser. A* **440,** 23 (1993).
9. R. de Ridder, J. van Landuyt, and S. Amelinckx, *Phys. Status Solidi A* **9,** 551 (1972).